

Zebrafish *short fin* mutations in connexin43 lead to aberrant gap junctional intercellular communication

Angela D. Hoptak-Solga^a, Kathryn A. Klein^b, Adam M. DeRosa^b, Thomas W. White^b,
M. Kathryn Iovine^{a,*}

^a Lehigh University, Department of Biological Sciences, 111 Research Drive, Iacocca B-217, Bethlehem, PA 18015, United States

^b Graduate Program in Genetics and The Department of Physiology & Biophysics, State University of New York, Stony Brook, NY 11794-8661, United States

Received 27 March 2007; revised 4 June 2007; accepted 15 June 2007

Available online 21 June 2007

Edited by Beat Imhof

Abstract Mutations in the zebrafish *connexin43* (*cx43*) gene cause the *short fin* phenotype, indicating that direct cell–cell communication contributes to bone length. Three independently generated *cx43* alleles exhibit short segments of variable sizes, suggesting that gap junctional intercellular communication may regulate bone growth. Dye coupling assays showed that all alleles are capable of forming gap junction channels. However, ionic coupling assays revealed allele-specific differences in coupling efficiency and gating. For instance, oocyte pairs expressing the weakest allele exhibited much higher levels of coupling than either of the strong alleles. Therefore, measurable differences in Cx43 function may be correlated with the severity of defects in bone length.

© 2007 Federation of European Biochemical Societies. Published by Elsevier B.V. All rights reserved.

Keywords: Gap junction; Cx43; Bone growth; Zebrafish; *short fin*

1. Introduction

Gap junctions serve as intercellular passageways for the exchange of small molecules (≤ 1200 Da in size), thereby facilitating direct communication between neighboring cells. Each gap junction channel consists of two hemichannels, or connexons. Each connexon contains six four-pass transmembrane spanning proteins called connexins. Interestingly, many connexin proteins seem to be required to fulfill the role of direct cell–cell communication. For example, there are 21 connexin genes in humans and 20 in the mouse [1]. The significance of gap junctional intercellular communication (GJIC) during development is evidenced by the large number of connexin mutations leading to human disease phenotypes [2,3]. In particular, mutations in human and mouse *CX43* cause oculodentodigital dysplasia (ODDD), a syndrome resulting in abnormalities of the craniofacial and distal limb skeleton as well as other pleiotropic phenotypes [4,5]. ODDD is transmitted as an autosomal dominant disease [4]. Mutations are typically missense mutations, which likely retain some level of function.

How might missense mutations affect the function of connexin proteins? *CX43* mutations linked to ODDD have been examined in heterologous assays [6–9]. The majority of *CX43* mutations retain the ability to assemble into gap junction plaques at the cell surface, suggesting that trafficking is not the primary cause for phenotypic variation (however, several mutant alleles result in reduced plaque formation). Indeed, defects in ionic and/or dye coupling have been revealed for all of the *CX43* mutants studied [6–9]. Therefore, the reduction in Cx43-mediated GJIC among these mutants may contribute to the development of ODDD-related phenotypes. Still, the underlying mechanism for the development of disease phenotypes remains unclear.

Mutations in zebrafish connexin genes have been identified only recently [10,11]. In particular, mutations in zebrafish *cx43* result in morphological abnormalities of the fin skeleton, suggesting that the function of *cx43* is conserved [10]. The original allele of *short fin* (*sof*^{b123}) exhibits reduced *cx43* gene expression and develops short fins due to defects in the length of bony fin ray segments. In addition to the original, non-coding sequence mutation in the *cx43* gene, three non-complementing ENU-induced mutations were identified (*sof*^{b7e1} coding for Cx43-F30V in the first transmembrane domain; *sof*^{b7e2} coding for Cx43-P191S in the second extracellular loop; *sof*^{b7e3} coding for Cx43-F209I in the fourth transmembrane domain). Previously, we found that the different missense mutations have different effects on segment length [10]. For example, homozygous Cx43-F209I alleles have only a slight effect on segment length and on fin length. In contrast, homozygous Cx43-F30V and Cx43-P191S alleles exhibit segments of similar length as the original allele (*sof*^{b123}). Since all alleles are adult viable, some level of function is predicted for each. However, as each missense mutation is found in the channel-forming region, effects on GJIC are anticipated.

The goal of this study is to determine if GJIC is affected in each mutant allele of zebrafish *cx43*, and further, if the severity of the defect is correlated with the *in vivo* segment length phenotype. For example, one possibility is that the efficiency of GJIC is directly related to segment length. We tested this hypothesis by monitoring the function of gap junctions using dye coupling and ionic coupling assays. Indeed, we found that the strong alleles of *cx43* (Cx43-F30V and Cx43-P191S) have more severe defects in coupling than the weakest allele (Cx43-F209I), which exhibits only moderate defects.

*Corresponding author. Fax: +1 610 758 4004.
E-mail address: mki3@lehigh.edu (M.K. Iovine).

2. Materials and methods

2.1. Generation of constructs for GJIC assays

The coding sequence from each allele (wild-type, *sof^{β7e1}* coding for Cx43-F30V, *sof^{β7e2}* coding for Cx43-P191S, and *sof^{β7e3}* coding for Cx43-F209I) was amplified using oligonucleotides with EcoRI sites engineered at the 5' ends (cx43-E2F TCGCAGAATTCGATGGGT-GACTGGAGTGCG); (cx43-E2R-CGACAGAATTCGGACGTC-CAGGTCATCAGG). Amplified products were subcloned into the EcoRI site of pEGFP-N1 (Clontech) and sequenced to ensure that additional errors were not introduced during amplification. The coding sequences were also subcloned into pCS2+. Alleles expressed in pEGFP-N1 were used for dye coupling assays in HeLa cells. Sense RNA transcribed from the pCS2+ vector was injected into *Xenopus* oocytes for ionic coupling assays.

2.2. Cell culture and transfection of HeLa cells

HeLa cells were grown in minimal essential medium supplemented with 10% fetal bovine serum, 0.1 mM non-essential amino acids, penicillin and streptomycin (Gibco-BRL). The cells were plated to 50% confluency in 35 mm dishes and transfected with 0.5 μg of plasmid DNA using the Effectene reagent (Sigma). Transfection efficiency was determined 24 h later by visualizing live cells for Cx43-EGFP expression with a fluorescence microscope.

2.3. Microinjection of HeLa cells using propidium iodide

Pairs of HeLa cells that had been transfected with each of the *cx43* alleles subcloned in the pEGFP-N1 vector were microinjected using the Eppendorf FemtoJet microinjector and Eppendorf InjectMan[®] NI2 micromanipulator. One cell from each pair was injected with propidium iodide (PI; 1 mg/mL, MW = 668.4) and a total of 50 cell pairs were injected. After transfer had proceeded for 15 min, the cells were viewed for fluorescence using a Nikon Eclipse TE2000-E microscope fitted with the Endow GFPBP (Zeiss) filter for the visualization of EGFP. The number of injected cells able to transfer dye was determined as a percentage in each of three experiments. The cells were determined to have successfully transferred dye if the dye was detectable in the non-injected cell of a pair. Three independent experiments were carried out, the percentage of cells that shared dye was determined per experiment, and the standard deviation was calculated. Student's *t*-tests were completed to determine if differences in dye coupling (between each mutant allele and wild-type Cx43) were significant.

2.4. In vitro transcription, oocyte microinjection and pairing

Wild-type and mutant *cx43* constructs were linearized using the NotI restriction site of pCS2+, and transcribed using the SP6 mMessage mMachine RNA protocol (Ambion, Austin, TX). Adult *Xenopus* females were anesthetized with ethyl 3-aminobenzoate methanesulfonate and ovarian lobes were surgically removed and digested for 2 h in a solution containing 50 mg/ml collagenase B, and 50 mg/ml hyaluronidase in modified Barth's medium (MB) without Ca²⁺. Stage V–VI oocytes were collected and injected first with 10 ng of antisense *Xenopus* Cx38 oligonucleotide to eliminate endogenous connexins [12,13]. Antisense oligonucleotide treated oocytes were then injected with wild-type Cx43, Cx43-F30V, Cx43-P191S, or Cx43-F209I cRNA transcripts (5 ng/cell), or H₂O as a negative control. The vitelline envelopes were removed in a hypertonic solution (200 mM aspartic acid, 10 mM HEPES, 1 mM MgCl₂, 10 mM EGTA, and 20 mM KCl at pH 7.4), and the oocytes were manually paired with the vegetal poles apposed in MB with Ca²⁺.

2.5. Dual-cell whole-cell voltage clamp

Gap junctional coupling between oocyte pairs was measured using the dual whole-cell voltage clamp technique [14]. Current and voltage electrodes (1.2 mm diameter, omega dot; Glass Company of America, Millville, NJ) were pulled to a resistance of 1–2 MΩ with a horizontal puller (Narishige, Tokyo, Japan) and filled with solution containing 3 M KCl, 10 mM EGTA, and 10 mM HEPES, pH 7.4. Voltage clamp experiments were performed using two GeneClamp 500 amplifiers controlled by a PC-compatible computer through a Digidata 1320A interface (Axon Instruments, Foster City, CA).

For measurements of junctional conductance, both cells in a pair were initially clamped at –40 mV to eliminate any transjunctional

potential. One cell was then subjected to alternating pulses of ±20 mV, while the current produced by the change in voltage was recorded in the second cell. The current delivered to the second cell was equal in magnitude to the junctional current, and the junctional conductance was calculated by dividing the measured current by the voltage difference, $G_j = I_j / (V_1 - V_2)$. To determine voltage-gating properties, transjunctional potentials (V_j) of opposite polarity were generated by hyperpolarizing or depolarizing one cell in 20 mV steps (range = ±120 mV) while clamping the second cell at –40 mV. Currents were measured at the end of the voltage pulse, at which time they approached steady-state (I_{jss}). Macroscopic conductance (G_{jss}) was calculated by dividing I_{jss} by V_j , normalized to the values determined at ±20 mV, and plotted against V_j . Data describing the relationship of G_{jss} as a function of V_j were analyzed using Origin 6.1 (Microcal Software, Northampton, MA) and fit to a Boltzmann relation of the form: $G_{jss} = (G_{jmax} - G_{jmin}) / (1 + \exp[A(V_j - V_0)]) + G_{jmin}$, where G_{jss} is the steady-state junctional conductance, G_{jmax} (normalized to unity) is the maximum conductance, G_{jmin} is the residual conductance at large values of V_j , and V_0 is the transjunctional voltage at which $G_{jss} = (G_{jmax} - G_{jmin}) / 2$. The constant $A = nq/kT$ represents the voltage sensitivity in terms of gating charge as the equivalent number (n) of electron charges (q) moving through the membrane, k is the Boltzmann constant, and T is the absolute temperature.

2.6. Electrophysiological recording of hemichannel currents

Macroscopic recordings of hemichannel currents were recorded from single *Xenopus* oocytes using a GeneClamp 500 amplifier controlled by a PC-compatible computer through a Digidata 1320 interface (Axon Instruments). pClamp 8.0 software (Axon Instruments) was used to program stimulus and data collection paradigms. To obtain hemichannel *I*–*V* curves, cells were initially clamped at –40 mV and subjected to 5 s depolarizing voltage steps ranging from –30 to +60 mV in 10 mV increments. The effects of calcium on hemichannel currents was analyzed by recording hemichannel currents from cells incubated in either MB media without calcium, or MB supplemented with 2 mM CaCl₂.

3. Results

3.1. All missense alleles form gap junction channels

Mutant connexins may affect the formation of gap junction channels by failing to assemble into connexons and/or failing to target to the plasma membrane [15,16]. To determine if any of the alleles of zebrafish Cx43 exhibit such defects, expression of EGFP-tagged alleles was examined in HeLa cells. Gap junction channels aggregate in plaques (~100–1000 channels) and are visualized as puncta or lines in areas where cells are in contact with one another. Wild-type zebrafish Cx43-EGFP as well as each mutant allele were identified in gap junction plaques at the plasma membranes of adjacent transfected cells (Fig. 1B), indicating that all three alleles are capable of assembly into connexons and targeting to the plasma membrane.

Next, the function of the Cx43 mutant alleles was examined using dye coupling assays. Propidium iodide (MW 668) was microinjected into one cell of a transfected pair and dye transfer was monitored. In addition to evaluating coupling of the zebrafish Cx43 alleles, the human variants P1 and P3 were also tested. These variants form gap junction plaques but do not permit dye coupling [17], and therefore served as negative controls. Dye was successfully transferred to neighboring cells in the majority of cell pairs for each zebrafish allele (and dye was not transferred in cells transfected with either human P1 or P3), suggesting that the assembled gap junctions are functional (Fig. 1). Differences in dye coupling compared to wild-type was not observed ($P = 0.81$ for Cx43-F30V; $P = 0.72$ for Cx43-P191S; $P = 0.67$ for Cx43-F209I). Therefore, zebrafish missense mutations in Cx43 retain coupling activity by this measure.

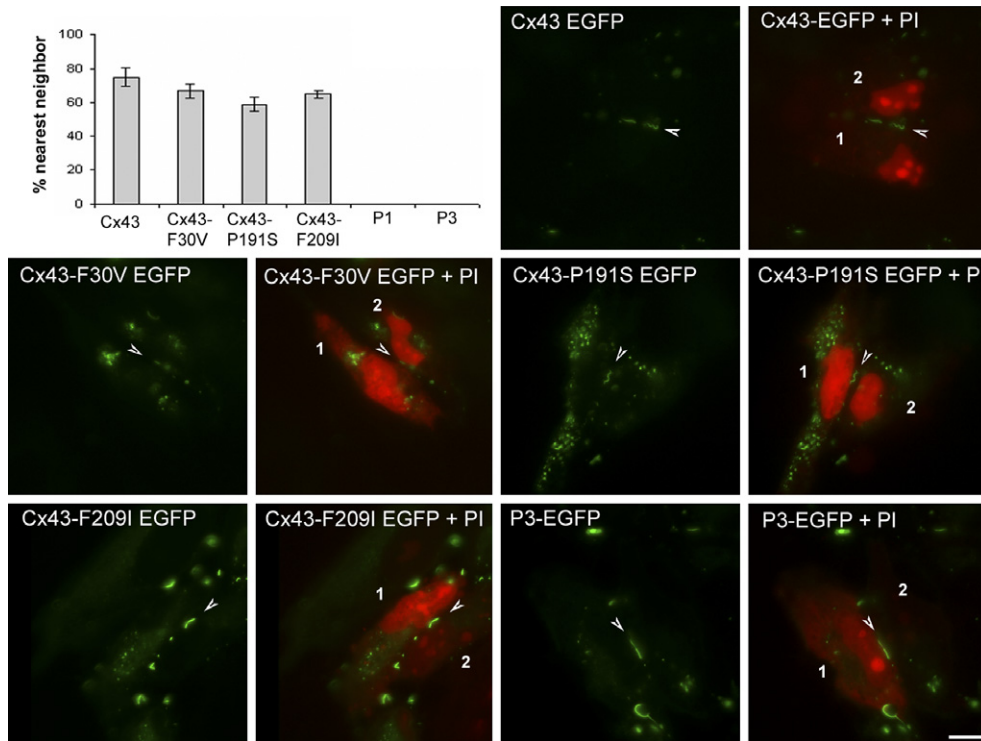


Fig. 1. Dye coupling of zebrafish Cx43 alleles. Top left: Dye coupling was evaluated by comparing the percent of cells that transfer dye in three separate experiments. Top right and bottom: Representative dye coupling results are shown for all zebrafish alleles and for the human variant Cx43-P3. Images are grouped so that EGFP fluorescence alone is shown on the left, and EGFP fluorescence plus propidium iodide (PI) staining is shown on the right. Single pairs of cells are shown and cells are labeled “1” or “2”. Arrowheads point to gap junction plaques. Scale bar = 10 μ m.

3.2. Differences in ionic coupling are detected among missense alleles

Next, GJIC was evaluated by ionic coupling assays. Using a paired *Xenopus* oocyte system, coupling efficiencies between cells were measured to determine if coupling occurs. Junctional conductance values for cells expressing the wild-type Cx43 allele as well as the Cx43-F30V, Cx43-P191S, and Cx43-F209I

alleles indicated the formation of functional gap junction channels, although with very different efficiencies (Fig. 2). Cells expressing the wild-type Cx43 allele were well coupled having

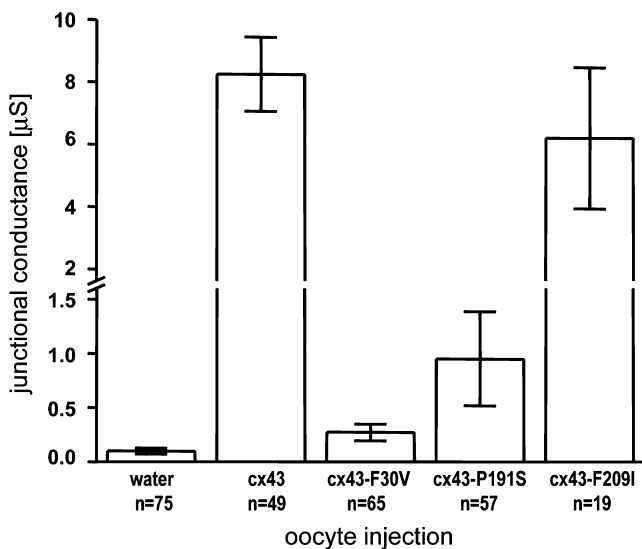


Fig. 2. Cx43 mutants exhibit defects in magnitude of ionic coupling. Junctional conductance values were measured by dual voltage clamp. Oocytes were injected with cRNA representing each Cx43 allele or water. Bars show means + S.D. of the number of pairs indicated.

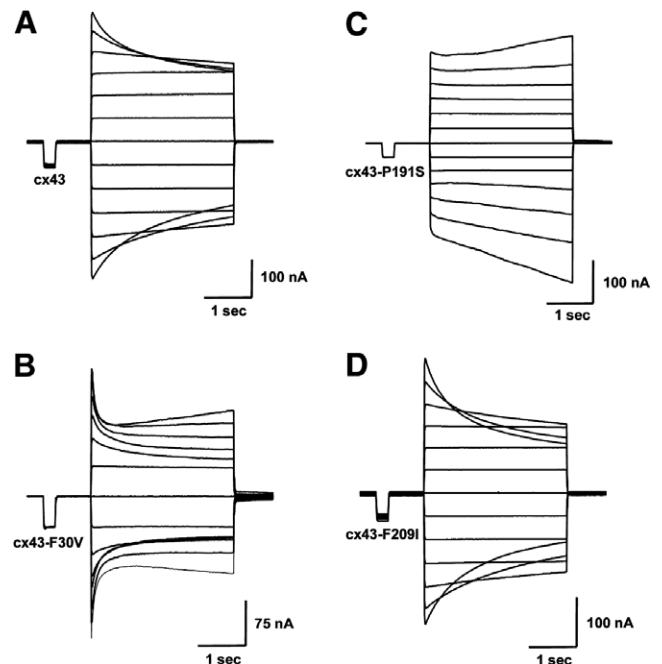


Fig. 3. Voltage-gating properties of channels expressing each of the mutant alleles of Cx43. Time-dependent decay of junctional currents (I_j) induced by transjunctional voltage (V_j) steps of 3 s duration applied in 20 mV increments.

a mean gap junctional conductance value of 8.24 μS . Oocyte pairs expressing Cx43-F209I were also well coupled with a mean conductance of 6.18 μS , a value not statistically different from wild-type Cx43 ($P = 0.39$, Student's t -test). In contrast, the stronger *sof* alleles Cx43-F30V and Cx43-P191S showed significantly lower levels of coupling than either Cx43 or Cx43-F209I ($P < 0.05$), with mean values of 0.27 and 0.95 μS , respectively. Although poorly coupled, both of these alleles induced electrical coupling that was significantly higher than background levels in water injected control cell pairs (0.09 μS , $P < 0.05$), but not statistically different from one another ($P = 0.10$). Thus, the least coupled cell pairs were found in oocytes expressing the strongest alleles (Cx43-F30V and Cx43-P191S) and the highest coupling was identified in oocytes expressing the weakest allele (Cx43-F209I).

3.3. Functional parameters are disturbed in strong mutant alleles of Cx43

The voltage-gating properties of Cx43 were monitored more carefully using junctional currents evoked by a series of transjunctional voltages between cell pairs expressing the wild-type Cx43 allele and each of the mutant alleles (Fig. 3). At high transjunctional voltages, currents decay rapidly in both wild-type Cx43 and Cx43-F209I, suggesting fast closure of the

channels. Further, Cx43-F209I channels appear slightly more voltage sensitive than Cx43 channels. In contrast, channels appear to open rather than close at higher voltages in cells expressing the strongest allele, Cx43-P191S. Cells expressing Cx43-F30V displayed the most unusual behavior. At lower transjunctional potentials they closed at lower voltages and more rapidly than wild-type Cx43. At higher transjunctional potentials, they showed an initial rapid closure followed by a slow opening. To analyze the equilibrium voltage-gating properties, steady-state conductance values were normalized, plotted against transjunctional voltage and fit to a Boltzmann equation (Fig. 4). This analysis revealed that Cx43-P191S and Cx43-F30V had a complex voltage/conductance relationship that could not be fit by the Boltzmann equation. In contrast, Cx43-F209I had properties similar to wild-type Cx43 with the most notable difference in the calculated value of minimum conductance ($G_{j\text{min}}$). Biophysically this result indicates that the stronger Cx43 alleles produce a more severe alteration of the gap junction channel structure. This altered structure of the channel may also result in different permeability to larger solutes such as signaling molecules.

Gap junction hemichannels have been implicated in normal and pathophysiological states [18–20] and the channel opening at higher transjunctional voltages displayed by Cx43-P191S

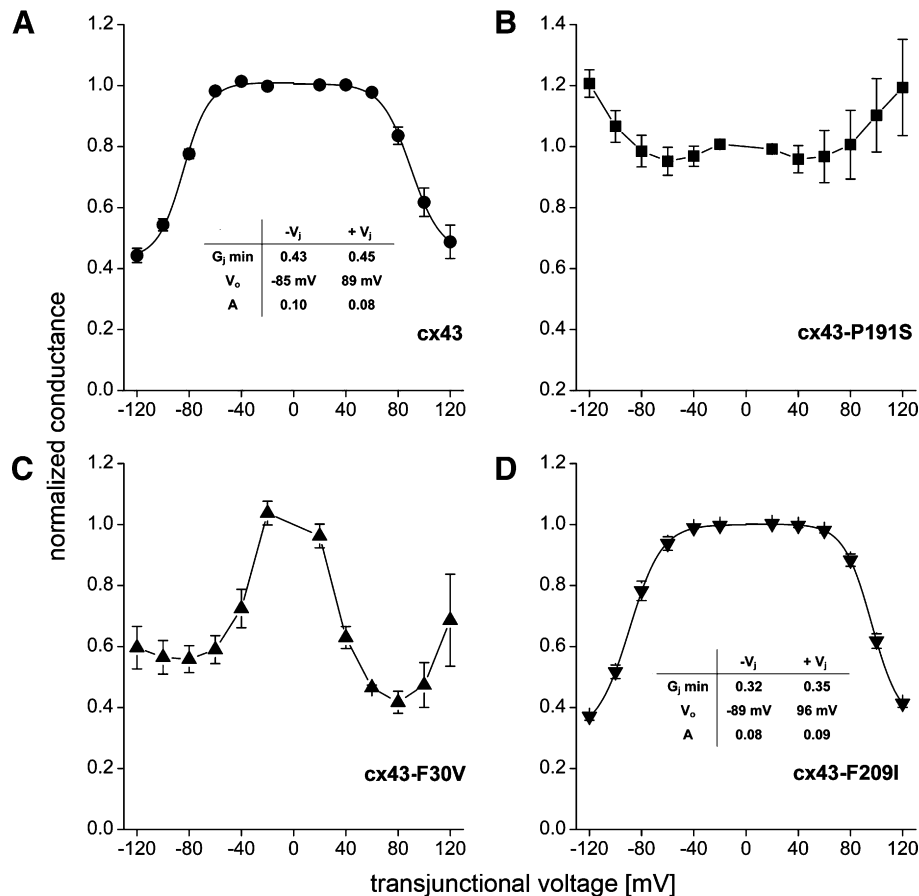


Fig. 4. Equilibrium gating properties of wild-type, Cx43-P191S, Cx43-F30V and Cx43-F209I channels. Steady-state junctional conductance (G_j) was normalized, plotted against transjunctional voltage (V_j) and fit to the Boltzmann equation. The smooth line shows the best fits to the Boltzmann equation whose parameters are inset for both wild-type Cx43 (A) and Cx43-F209I (D). Both wild-type and Cx43-F209I channels exhibited similar equilibrium gating properties. Conversely, Cx43-F30V (C), and Cx43-P191S (B) channels displayed marked differences in steady-state voltage dependence that could not be fit by the Boltzmann equation. Data are mean \pm S.E. $N = 3$ for all conditions tested.

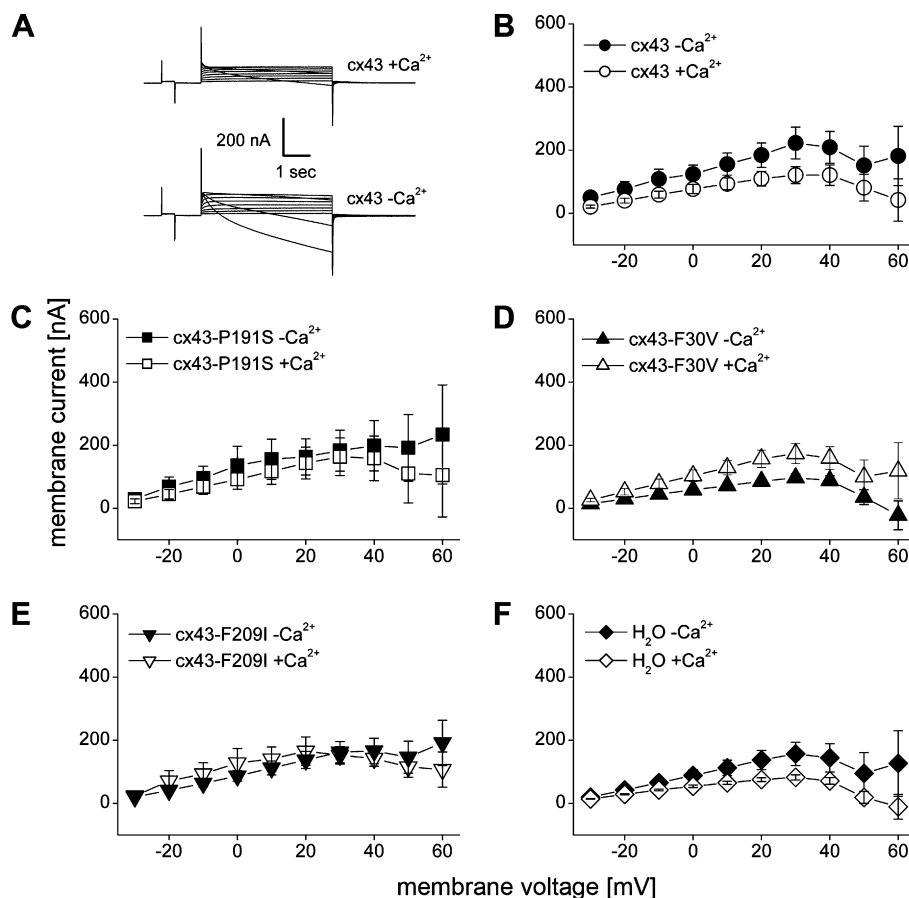


Fig. 5. Cx43 mutants have unaltered hemichannel activity in *Xenopus* oocytes. (A) Oocytes expressing wild-type Cx43 were subjected to voltage pulses ranging from -30 to $+60$ mV in 10 mV steps in the presence (top) or absence (bottom) of 2 mM CaCl_2 . Representative traces for both conditions displayed negligible membrane currents. (B) Steady-state currents in wild-type Cx43 injected cells were plotted as a function of membrane voltage in both the presence (open circles) and absence of CaCl_2 (closed circles). Currents for Cx43-P191S (C), Cx43-F30V (D) and Cx43-F209I (E) were similar to those observed in wild-type Cx43 injected cells at all voltages analyzed in the presence (open symbols) and absence of CaCl_2 (closed symbols). (F) Water injected control cells also failed to induce substantial membrane currents. $n = 10$ – 16 cells per condition. Data are the mean \pm S.E.M.

and Cx43-F30V may have included contributions from a novel form of hemichannel activity resulting from these two mutations. To test this possibility, single oocytes were subjected to depolarizing voltage pulses and membrane currents were recorded (Fig. 5). Wild-type Cx43 injected oocytes displayed negligible current flow over a range of voltages from -30 to $+60$ mV. When mean steady-state currents were plotted as a function of membrane potential all oocytes displayed small currents at all voltages tested, regardless of which cRNA was injected. These data show that the unusual gating behavior of the strongest alleles was attributable to changes in gap junctional activity rather than an activation of hemichannels.

4. Discussion

4.1. Cx43 function is correlated with bony segment length

In this report we monitored GJIC in Cx43 missense alleles using dye coupling and ionic coupling assays. We found that all three alleles are capable of forming functional gap junction plaques by two tests: dye coupling of EGFP-tagged alleles in HeLa cell assays and positive junctional conductance of untagged alleles in paired oocytes. We further show that Cx43-

F209I, the allele with the least severe segment length phenotype in vivo, exhibits high junctional conductance and voltage-gating properties similar to wild-type Cx43. In contrast, the more severe Cx43-F30V and Cx43-P191S alleles have very low junctional conductance and aberrant voltage-gating properties. Hemichannel activity does not account for the observed differences.

The severe defects in junctional conductance for Cx43-F30V and Cx43-P191S are in apparent contrast with the dye coupling results, which indicate that the mutant channels function as well as wild-type Cx43. However, the dye coupling assay is strictly qualitative, indicating only when some dye is shared but not how much or at what rate. Therefore, it may not be possible to distinguish between functional and moderately functional gap junction channels. Indeed, as each of the tested alleles result in homozygous viable mutations in vivo, it stands to reason that gap junctional communication is not completely abolished.

Since each missense mutation of *cx43* is found in the area comprising the channel [10], we hypothesized that defects in GJIC may be correlated with segment length. Indeed, this appears to be the case. Therefore, the trend with three mutant alleles provides support for our hypothesis that GJIC via Cx43 gap junctions may contribute to normal segment growth.

4.2. Zebrafish may be used as a model to examine the function of *Cx43* missense mutations

The mechanism by which missense mutations in connexin proteins leads to disease phenotypes is unclear. In particular, there does not appear to be a correlation between the location of the *CX43* mutations and the severity of observed ODDD phenotypes [4]. Further, there does not appear to be a correlation between channel activity and the severity/type of symptoms [6–8]. Patients with neurological symptoms may express mutant channels with complete or incomplete abrogation of coupling, and similar findings are true for other ODDD phenotypes. Indeed, the large number of pleiotropic phenotypes and the significant variation in the severity of ODDD symptoms likely contributes to the difficulties in identifying straight-forward structure–function–phenotypic correlations for mutations in human *CX43*.

In contrast to the complexity of the human and mouse *CX43* disease phenotypes, the zebrafish *cx43* alleles were identified as adult viable mutations, resulting in animals with milder phenotypes. While it is likely that pleiotropic phenotypes are present in *sof* animals, these phenotypes are likely more subtle (and other tissues have not yet been examined in detail for *cx43*-specific defects). Thus, the zebrafish *cx43* mutants provide an opportunity to examine the effects of *cx43* mutations on a single, relatively simple structure. Here we find a direct correlation between the strength of the phenotype *in vivo* and function in heterologous assays. The generation of additional alleles will permit a detailed analysis of *cx43* disease-related phenotypes for bone growth (and perhaps for other tissues that rely on *cx43* function, such as the heart). These results will be applicable to *Cx43* function in other animals, and to connexin function in general.

Acknowledgments: The authors thank Lynne Cassimeris for sharing tissue culture facilities and use of the Eppendorf microinjector system. Matthias Falk provided the P1 and P3 human *Cx43* variants. We thank Matthias Falk and Michael Burger for critical reading of the manuscript. This work was funded by grants supporting M.K.I. (HD047737) and T.W.W. (EY13163, DC06652).

References

- [1] Sohl, G. and Willecke, K. (2004) Gap junctions and the connexin protein family. *Cardiovasc. Res.* 62, 228–232.
- [2] Laird, D.W. (2006) Life cycle of connexins in health and disease. *Biochem. J.* 394, 527–543.
- [3] White, T.W. and Paul, D.L. (1999) Genetic diseases and gene knockouts reveal diverse connexin functions. *Annu. Rev. Physiol.* 61, 283–310.
- [4] Paznekas, W.A. et al. (2003) Connexin 43 (GJA1) mutations cause the pleiotropic phenotype of oculodentodigital dysplasia. *Am. J. Hum. Genet.* 72, 408–418.
- [5] Flenniken, A.M. et al. (2005) A Gja1 missense mutation in a mouse model of oculodentodigital dysplasia. *Development* 132, 4375–4386.
- [6] Seki, A., Duffy, H.S., Coombs, W., Spray, D.C., Taffet, S.M. and Delmar, M. (2004) Modifications in the biophysical properties of connexin43 channels by a peptide of the cytoplasmic loop region. *Circ. Res.* 95, e22–e28.
- [7] Shibayama, J., Paznekas, W., Seki, A., Taffet, S., Jabs, E.W., Delmar, M. and Musa, H. (2005) Functional characterization of connexin43 mutations found in patients with oculodentodigital dysplasia. *Circ. Res.* 96, e83–e91.
- [8] Roscoe, W. et al. (2005) Oculodentodigital dysplasia-causing connexin43 mutants are non-functional and exhibit dominant effects on wild-type connexin43. *J. Biol. Chem.* 280, 11458–11466.
- [9] Lai, A., Le, D.N., Paznekas, W.A., Gifford, W.D., Jabs, E.W. and Charles, A.C. (2006) Oculodentodigital dysplasia connexin43 mutations result in non-functional connexin hemichannels and gap junctions in C6 glioma cells. *J. Cell Sci.* 119, 532–541.
- [10] Iovine, M.K., Higgins, E.P., Hindes, A., Coblitz, B. and Johnson, S.L. (2005) Mutations in connexin43 (GJA1) perturb bone growth in zebrafish fins. *Dev. Biol.* 278, 208–219.
- [11] Watanabe, M., Iwashita, M., Ishii, M., Kurachi, Y., Kawakami, A., Kondo, S. and Okada, N. (2006) Spot pattern of leopard Danio is caused by mutation in the zebrafish connexin41.8 gene. *EMBO Rep.* 7, 893–897.
- [12] Barrio, L.C., Suchyna, T., Bargiello, T., Xu, L.X., Roginski, R.S., Bennett, M.V. and Nicholson, B.J. (1991) Gap junctions formed by connexins 26 and 32 alone and in combination are differently affected by applied voltage. *Proc. Natl. Acad. Sci. USA* 88, 8410–8414.
- [13] Bruzzone, R., Haefliger, J.A., Gimlich, R.L. and Paul, D.L. (1993) Connexin40, a component of gap junctions in vascular endothelium, is restricted in its ability to interact with other connexins. *Mol. Biol. Cell* 4, 7–20.
- [14] Spray, D.C., Harris, A.L. and Bennett, M.V. (1981) Equilibrium properties of a voltage-dependent junctional conductance. *J. Gen. Physiol.* 77, 77–93.
- [15] Ressayre, C. and Bruzzone, R. (2000) Connexin channels in Schwann cells and the development of the X-linked form of Charcot-Marie-Tooth disease. *Brain Res. Brain Res. Rev.* 32, 192–202.
- [16] Abrams, C.K., Oh, S., Ri, Y. and Bargiello, T.A. (2000) Mutations in connexin 32: the molecular and biophysical bases for the X-linked form of Charcot-Marie-Tooth disease. *Brain Res. Brain Res. Rev.* 32, 203–214.
- [17] Lagree, V., Brunschwig, K., Lopez, P., Gilula, N.B., Richard, G. and Falk, M.M. (2003) Specific amino-acid residues in the N-terminus and TM3 implicated in channel function and oligomerization compatibility of connexin43. *J. Cell Sci.* 116, 3189–3201.
- [18] Saez, J.C., Retamal, M.A., Basilio, D., Bukauskas, F.F. and Bennett, M.V. (2005) Connexin-based gap junction hemichannels: gating mechanisms. *Biochim. Biophys. Acta* 1711, 215–224.
- [19] Jiang, J.X. and Gu, S. (2005) Gap junction- and hemichannel-independent actions of connexins. *Biochim. Biophys. Acta* 1711, 208–214.
- [20] Gerido, D.A., Derosa, A.M., Richard, G. and White, T.W. (2007) Aberrant hemichannel properties of *Cx26* mutations causing skin disease and deafness. *Am. J. Physiol. Cell Physiol.*